University of Reading

U.K. climate projections: Summer daytime and nighttime urban heat island changes in England's major cities

Article

Accepted Version

Eunice Lo, Y. T., Mitchell, D. M., Bohnenstengel, S. I., Collins, M., Hawkins, E. ORCID: https://orcid.org/0000-0001-9477-3677, Hegerl, G. C., Joshi, M. and Stott, P. A. (2020) U.K. climate projections: Summer daytime and nighttime urban heat island changes in England's major cities. Journal of Climate, 33 (20). pp. 9015-9030. ISSN 0894-8755 doi: 10.1175/JCLI-D-19-0961.1 Available at https://centaur.reading.ac.uk/93070/

It is advisable to refer to the publisher's version if you intend to cite from the work. See Guidance on citing.
Published version at: http://dx.doi.org/10.1175/JCLI-D-19-0961.1
To link to this article DOI: http://dx.doi.org/10.1175/JCLI-D-19-0961.1

All outputs in CentAUR are protected by Intellectual Property Rights law, including copyright law. Copyright and IPR is retained by the creators or other copyright holders. Terms and conditions for use of this material are defined in the End User Agreement.

www.reading.ac.uk/centaur

University of Reading

CentAUR

Central Archive at the University of Reading

Reading's research outputs online

UK Climate Projections: Summer daytime and night-time urban heat island changes in England's major cities

Y. T. Eunice Lo*; Daniel M. Mitchell

School of Geographical Sciences, University of Bristol, Bristol, UK

Sylvia I. Bohnenstengel

MetOffice@Reading, Department of Meteorology, University of Reading, Reading, UK

Mat Collins

College of Engineering, Mathematics and Physical Sciences, University of Exeter, Exeter, UK

Ed Hawkins

National Centre for Atmospheric Science, Department of Meteorology, University of Reading, Reading, UK

Gabriele C. Hegerl

School of Geosciences, University of Edinburgh, Edinburgh, UK

Manoj Joshi

Climatic Research Unit, School of Environmental Sciences, University of East Anglia, UK

Peter A. Stott

Met Office Hadley Centre, Exeter, UK

* *Corresponding author address:* School of Geographical Sciences, University of Bristol, Bristol BS8 1SS, UK

E-mail: eunice.lo@bristol.ac.uk

ABSTRACT

In the UK where 90% of residents are projected to live in urban areas by 2050, projecting changes in urban heat islands (UHIs) is essential to municipal adaptation. Increased summer temperatures are linked to increased mortality. Using the new regional UK Climate Projections, UKCP18-regional, we estimate the 1981–2079 trends in summer urban and rural near-surface air temperatures, and UHI intensities during day and at night in the 10 most populous built-up areas in England. Summer temperatures increase by 0.45–0.81°C per decade under RCP8.5, depending on the time of day and location. Night-time temperatures increase more in urban than rural areas, enhancing the night-time UHI by 0.01–0.05°C per decade in all cities. When these upward UHI signals emerge from 2008–2018 variability, positive summer night-time UHI intensities of up to 1.8°C are projected in most cities. However, we can prevent most of these upward night-time UHI signals from emerging by stabilising climate to the Paris Agreement target of 2°C above pre-industrial levels. In contrast, daytime UHI intensities decrease in nine cities, at rates between -0.004 and -0.05°C per decade, indicating a trend towards a reduced daytime UHI effect. These changes reflect different feedbacks over urban and rural areas and are specific to UKCP18-regional. Future research is important to better understand the drivers of these UHI intensity changes.

1. Introduction

Increased exposure to high temperatures and, therefore, increased levels of heat-related mortality are projected in a warming world (Lo et al. 2019; Vicedo-Cabrera et al. 2018). Urban inhabitants are generally more susceptible to heat stress due to the urban heat island effect (Fischer et al. 2012; Heaviside et al. 2016). An urban heat island is characterised by higher near-surface air or surface skin temperatures in a given urban area compared to its rural surroundings. This study focuses on the air urban heat island (UHI) effect because it has direct relevance to heat stress.

Urban areas tend to be densely built with structures such as buildings and paved roads. Narrow streets flanked by tall buildings on both sides are a common sight, forming urban canyons that have large surface areas for daytime heat absorption (Kershaw et al. 2010). Construction materials such as concrete and asphalt have low albedo. The thermal properties and large surface areas of urban structures lead to a high thermal inertia (Erell and Williamson 2007; Bohnenstengel et al. 2011), meaning that urban structures absorb and store heat during the day and release it at night (Yamamoto 2006; Kershaw et al. 2010; Schlünzen and Bohnenstengel 2016). With densely built structures, urban areas tend to lack vegetation. On the contrary, rural areas tend to be less densely built than urban areas. Natural land covered in soil and vegetation has lower thermal inertia, higher albedo and often more moisture than urban areas. These urban/rural differences tend to lead to the formation of an UHI.

During the day, net incoming solar radiation increases heat storage in the urban canopy. The stored heat leads to an upward directed sensible heat flux that warms the urban boundary layer once surface temperatures exceed air temperatures. With lower thermal inertia, the upward sensible heat flux increases earlier in the day in rural areas (Oke 1987; Kershaw et al. 2010; Sachindra et al. 2016; Bohnenstengel et al. 2011). At night, the urban environment maintains a positive upward

sensible heat flux until urban surface temperatures drop below air temperatures. On the other hand, the sensible heat flux in the rural surroundings quickly decreases due to their small thermal inertia. This phase shift in sensible heat flux is one of the causes of air temperature differences between urban and rural areas (Bohnenstengel et al. 2011, 2014).

Paved surfaces and reduced vegetation in urban areas limit latent heat loss through evapotranspiration, increasing the upward sensible heat flux that warms the urban boundary layer (Oke 1987; Kershaw et al. 2010). Moreover, urban canyons increase roughness and reduce average wind speeds, reducing total turbulent heat loss (Oke 1987; Wilby 2003). In addition, anthropogenic heat from energy use, traffic and industrial processes (Bohnenstengel et al. 2014; Allen et al. 2011), and urban air pollution can contribute to an UHI depending on the time of day (Oke 1987; Wilby 2003).

The UHI effect has been observed around the world (Sachindra et al. 2016; Wilby 2003; Cui and De Foy 2012; Basara et al. 2010; Tan et al. 2010; Erell and Williamson 2007). It is most pronounced under clear skies and low wind conditions, when urban/rural differences in stored energy, net longwave radiation loss and turbulent heat loss are greatest (Oke 1987; Erell and Williamson 2007). The UHI effect is commonly quantified by the UHI intensity, which in this study is the near-surface air temperature difference between an urban site and a rural site. In the UK, UHI intensities of over 7°C in central London (Wilby 2003), up to 5°C in Manchester (Smith et al. 2011), and nearly 5°C in Birmingham (Heaviside et al. 2015) were recorded during summer periods. All these observation-based studies reported maximum UHI intensities at night, revealing a diurnal cycle of the UHI effect that is consistent with the literature (Oke 1987).

Using climate model simulations, Fischer et al. (2012) showed that summer urban air tended to be warmer and drier than rural air in regions including North Europe. The effect of this was a positive urban/rural contrast in heat stress that was most pronounced at night, highlighting the risk

of heat-related morbidity and mortality in urban population. Indeed, 52% of heat-related deaths in the West Midlands, UK, during the August 2003 heatwave could be attributed to the UHI effect (Heaviside et al. 2016). An increase in high heat stress occurrences (Fischer et al. 2012) and mortality (Heaviside et al. 2016) is projected for urban areas in a warming climate.

Apart from heat stress, UHIs can induce mesoscale atmospheric circulations, typically characterised by convergence in the lower part of the planetary boundary layer and divergence in the upper part if a UHI is positive (Zhang et al. 2014). The strength of an UHI-induced circulation depends on the UHI intensity and background wind conditions. Vukovich et al. (1979) reported high surface ozone concentrations in the zone of convergence when UHI circulation persisted in St. Louis, USA, demonstrating links between UHIs and the formation and concentration of this air pollutant (Lee 1979). In Paris, Sarrat et al. (2006) concluded that the UHI significantly modified the spatial distribution and availability of ozone and nitrogen oxide during an anticyclonic episode in 1999. Indeed, links between UHI-induced mesoscale winds and severe air pollution in urban areas were supported by mathematical modelling (Agarwal and Tandon 2010). Conversely, mitigation of the UHI in Stuttgart, Germany, was found to reduce vertical dilution of urban primary pollutants such as nitric oxide and carbon monoxide, increasing their concentrations (Fallmann et al. 2016). Air pollution has a potential confounding effect on heat-related mortality (Rainham and Smoyer-Tomic 2003).

In a warming climate, projected increases in urban and rural temperatures would affect human heat stress and potentially the effect of UHI. Such changes need to be quantified because 68% of the world's population (United Nations 2018) and 90% of the UK's population (United Nations DESA/Population Division 2018) are projected to live in urban areas by 2050. Using extrapolation and statistical downscaling techniques, studies estimated an increase in UHI intensity to 2.4°C in Manchester by the end of this century (Levermore et al. 2018) and a 0.5°C increase in summer

night-time UHI intensity in London between the 1960s and the 2050s (Wilby 2008). However, another study that coupled a regional climate model to an urban land surface scheme found a 0.1°C decrease in summer daytime UHI intensity and an unaltered summer night-time UHI intensity in London between 1971–1990 and 2041–2060 (Mccarthy et al. 2012).

The UK Met Office produce a new set of UK climate projections every few years to provide the most up-to-date assessment of climate change over the 21st century. Mainly designed for the UK and peer reviewed, these projections are one of the most reputable datasets available for the UK. While the previous generation, UKCP09, did not include urban effects (Murphy et al. 2009), the newest regional UK climate projections (UKCP18-regional) include an urban land surface type for the first time (Murphy et al. 2018, 2009). This provides a new opportunity for us to assess future urban and rural temperature and UHI intensity changes in the UK. Here, we estimate trends in summer daytime and night-time temperatures in urban and rural areas, as well as the resulting trends in UHI intensities in the 10 most populous built-up areas in England; Greater London, Greater Manchester, West Midlands, West Yorkshire, Liverpool, South Hampshire, Tyneside, Nottingham, Sheffield and Bristol; in the period 1981–2079.

We investigate whether future summer urban and rural temperatures, and UHI intensities in these built-up areas would be statistically significantly different from their most recent (2008–2018) values, taking climate variability into account. By estimating at what levels of global mean warming these changes in temperature or UHI intensity might emerge from variability, we compare our emergence results to the Paris Agreement's 1.5 and 2°C temperature targets (UNFCCC 2015) and the 3°C warming above pre-industrial levels that current nationally determined contributions (NDCs) may imply (Rogelj et al. 2016).

2. Materials and Methods

a. HadUK-Grid

To examine the historical UKCP18-regional simulations of urban and rural temperatures and the UHI effect in England, we make use of the gridded climate observations for the UK, HadUK-Grid (Hollis et al. 2019). HadUK-Grid is a new collection of gridded datasets created by the UK Met Office based on meteorological station data. Datasets of various climate variables dating back to as early as the second half of the 19th century are available at horizontal resolutions of up to 1 km. Please refer to Hollis et al. (2019) for the details of quality control and gridding of the data.

Due to a lack of sub-daily temperature data from HadUK-Grid and indeed UKCP18-regional, we investigate changes and trends in summer daytime and night-time UHI intensities based on daily maximum and minimum air temperatures (*tasmax* and *tasmin*) in June, July and August (JJA) throughout this study. We use the 1981–2017 JJA daily *tasmax* and *tasmin* data from HadUK-Grid at 12 km resolution for direct comparison with UKCP18-regional and for bias correction.

b. UKCP18-regional

UKCP18-regional is a set of climate simulations over a European domain (20.51–66.89°N, 47.59°W–68.54°E) for the period 1980–2080, with projections beyond 2005 based on the RCP8.5 scenario (Murphy et al. 2018). Being a high emissions scenario, RCP8.5 was chosen by the Met Office to identify climate change signals against natural variability in the near future. This way, climate risks can be assessed in a precautionary approach. UKCP18-regional has a horizontal resolution of 12 km that resolves finer features than its predecessor, UKCP09 (Murphy et al. 2009).

UKCP18-regional consists of 12 perturbed parameter ensemble members of the regional atmospheric model HadREM3-GA7-05, each of which was driven by the corresponding global simula-

tion (at 60 km resolution) of a new UK Met Office coupled atmosphere-ocean model, HadGEM3-GC3.05 (Murphy et al. 2018). This global climate model generally simulates higher global mean temperatures than the observations (Cowtan and Way 2014) for the period 2000–2017 (Murphy et al. 2018). For future years, the HadGEM3-GC3.05 ensemble projects higher global mean temperatures than most selected CMIP5 models under RCP8.5 (Murphy et al. 2018; Taylor et al. 2012). This suggests a higher equilibrium climate sensitivity in the model, which can be explained by a weaker shortwave negative cloud feedback in the midlatitudes (Bodas-Salcedo et al. 2019).

The twelve UKCP18-regional ensemble members were selected by the Met Office based on criteria that maximised the ensemble spread in global aerosol forcing, climate feedback strength, and model parameters in the convection, gravity wave drag, boundary layer, cloud, aerosols and land surface schemes (Murphy et al. 2018). The Met Office also validated the members' historical performance in European climatology, Atlantic meridional overturning circulation strength and northern hemisphere surface temperature. Nevertheless, since they were all driven by HadGEM3-GC3.05, they sample the warmer end of probabilistic future projections as compared with CMIP5 (Murphy et al. 2018).

UKCP18-regional provides a new opportunity to study the urban effects on UK climate in the 21st century. Urban effects are represented as one of nine land surface types in the model. A tiling approach is used to calculate the surface energy balance separately for each sub-grid scale surface type in each grid box. An aggregated surface energy balance is then calculated based on these sub-grid scale fluxes (Best et al. 2011). The one-tile urban scheme in UKCP18-regional uses a bulk representation for urban areas by introducing a large thermal inertia, and it radiatively couples the urban surface and the soil (Best 2005). Although urban characteristics such as canopy

heat capacity (2.8×10^5 J K^{-1} m^{-2}) and roughness lengths for heat and momentum do not vary spatially in this scheme (Best et al. 2011), urban land cover fraction does.

Figure 1 shows the urban fraction in each 12 km UKCP18-regional grid box covering England and Wales on the Ordnance Survey's British National Grid. These urban fractions do not change over time in the simulations. Grid boxes with elevated urban fractions are mainly located in the 10 most populous built-up areas (BUAs) in England and Wales defined by the Office for National Statistics (Office for National Statistics 2013) (Figure 1). We identify urban and rural grid boxes with the urban fractions and study the UHI effect in the BUAs shown in Figure 1 . Hereafter, we refer to the BUAs by the main cities therein (city names and locations are indicated on Figure 1). In descending order of 2016 population estimates, the included BUAs (cities) are: Greater London (London), Greater Manchester (Manchester), West Midlands (Birmingham), West Yorkshire (Leeds), Liverpool (Liverpool), South Hampshire (Southampton), Tyneside (Newcastle), Nottingham (Nottingham), Sheffield (Sheffield) and Bristol (Bristol). Please see Table 1 for more details.

c. EURO-CORDEX

Although our main focus is the new UKCP18-regional simulations, we include UHI projections from the European branch of the Coordinated Regional Downscaling Experiment (EURO-CORDEX) (Jacob et al. 2014) in Section 4 to aid discussion of our results. EURO-CORDEX is an internationally coordinated framework that provides regional climate projections for the same European domain as UKCP18-regional. Regional climate models (RCMs) are driven by various CMIP5 global climate models (GCMs) within EURO-CORDEX, producing climate data at 50 km and $\sim$12 km horizontal resolutions under different scenarios including RCP8.5 (Jacob et al. 2014).

Here, we use daily historical and RCP8.5 simulations of *tasmax* and *tasmin* at 12 km resolution from the GCM-RCM pairs from three modelling groups — the Met Office Hadley Centre

(MOHC), the Institut Pierre-Simon Laplace (IPSL) and the Max-Planck-Institut für Meteorologie (MPI-M). The included RCMs are MOHC's HadREM3-GA7-05, IPSL's WRF381P and MPI-M's REMO2009 (Jacob et al. 2012). These RCMs are respectively driven by HadGEM2-ES (Jones et al. 2011), IPSL-CM5A-MR (Dufresne et al. 2013) and MPI-ESM-LR (Giorgetta et al. 2013). The MOHC and IPSL models have one simulation each, whereas the MPI-M model has 2 ensemble members.

d. UHI intensity

We define UHI intensity as the near-surface air temperature (at 1.5 m) difference between urban and rural grid boxes in the same area. For each included city, we define a 5-grid by 5-grid box centred on its city centre, the location of which is indicated on Figure 1. Based on the urban fractions in UKCP18-regional as shown in Figure 1, the two grid boxes with the highest urban fractions in this box are identified as urban, whereas the two grid boxes with the lowest urban fractions are identified as rural. We use this definition because it can be applied to all chosen cities even though they have substantially different sizes and degrees of urbanisation (Figure 1). Table 1 lists the urban fractions in the selected grid boxes for all cities. All urban grid boxes have an urban fraction higher than 0.15, whereas all rural grid boxes have an urban fraction substantially lower than this threshold. Since the rural grid boxes in the top five cities are not entirely rural (urban fraction = 0), we may be underestimating the UHI intensity in the largest cities.

For each included city, the urban temperature, T_{urban}, is the average temperature across the two urban grid boxes; whereas the rural temperature, T_{rural}, is the average temperature across the two rural grid boxes. The UHI intensity of a city (in °C) is given by: UHI intensity = T_{urban} - T_{rural}. Representing urban areas by two grid boxes overestimate the size of the smaller cities (Table 1), so

we may be underestimating the UHI intensity in these cities. Using one or six grid boxes instead of two does not alter our main results (not shown).

We focus on summer months, i.e. June, July and August, or JJA, because these are months when heatwaves happen. We also investigate how UHI intensity may change in each city on its annual three consecutive warmest days, i.e. the three consecutive days over which average daily *tasmax* is the highest among all three-day periods in a year in each 5-grid by 5-grid box centred on a city centre (see above). Identifying warmest periods via *tasmax* over three consecutive days is similar to the Met Office's official definition of a heatwave (UK Met Office 2019). We assume the warmest days in the 5-grid by 5-grid boxes are representative of the warmest days over individual urban and rural grid boxes therein (Fenner et al. 2019).

For each year in 1981–2079 and for each ensemble member, we calculate the average summer (JJA) and "warmest days" daytime and night-time UHI intensities from daily *tasmax* and *tasmin* in identified urban and rural grid boxes. We also compute the ensemble averages. We find trends in daytime and night-time T_{urban}, T_{rural} and UHI intensities by linearly regressing the annual temperature or UHI intensity values against year via ordinary least squares regression.

e. Bias correction

Although the twelve UKCP18-regional ensemble members simulate higher global mean temperatures than the observations (Section 2b); they, on average, simulate lower JJA *tasmax* and *tasmin* but larger warming trends than HadUK-Grid for most of the UK in 1981–2017 (Figure A1). Exceptions are in *tasmin* in South East England and North West Scotland, where the UKCP18-regional ensemble mean temperatures are higher than the observed values in HadUK-Grid. The cool biases in summer temperatures in most parts of the UK are consistent with the Met Office's evaluation of the model against the National Climate Information Centre's data from 1981–2000 (Murphy et al.

2018), and they are associated with increased cloud cover in the regional model (Murphy et al. 2018).

The 12-member UKCP18-regional ensemble adequately samples HadUK-Grid temperatures except for *tasmin* in the London area and *tasmax* in Scotland (hatching in Figure A1 indicates areas where HadUK-Grid falls outside of the UKCP18-regional ensemble spread). However, different model biases between urban and rural grid boxes lead to biases in UHI intensity. For example, a smaller cool bias in *tasmax* and a larger warm bias in *tasmin* in central London compared to its surroundings (Figure A1) lead to an overestimation of both daytime and night-time UHI intensities in London (Figures A2 and A3). Indeed, UKCP18-regional generally overestimates summer UHI intensities in the cities of interest in 1981–2017, with night-time UHI biases more pronounced than daytime biases (Figures A2 and A3).

To bias correct, we find the offset in 1981–2017 mean JJA *tasmax* and *tasmin* between HadUK-Grid and each UKCP18-regional ensemble member in each grid box. Assuming these offsets do not change over time, we add them to the corresponding *tasmax* and *tasmin* simulations in UKCP18-regional for the whole period of 1981–2079. In other words, we shift the mean temperature and, therefore, UHI intensity in individual UKCP18-regional ensemble members to match the 1981–2017 mean in HadUK-Grid. Correcting only the mean is reasonable here because (i) the biases in daytime and night-time UHI intensities in UKCP18-regional appear to be close to constant over time in 1981–2017 (Figures A2 and A3), and (ii) the standard deviations in *tasmax* and *tasmin* are similar between HadUK-Grid and UKCP18-regional (not shown). All UKCP18-regional results in the remainder of this study are based on bias-corrected data.

By removing the mean bias in temperature, we preserve the raw UHI trends in UKCP18-regional. All members of the UKCP18-regional ensemble underestimate the summer daytime UHI trend for Liverpool, Southampton, Newcastle and Bristol; and overestimate the trend for

Nottingham in 1981–2017 (bottom left panel of Figure A4). For night-time UHI, the whole UKCP18-regional ensemble overestimate the trend for Birmingham (bottom right panel of Figure A4). These biases should be taken into account when interpreting the trend results for these cities.

The EURO-CORDEX models simulate a wide range of UHI intensity averages and trends in the period 1981–2017 (Figure A4), showing larger biases than UKCP18-regional in some cases. We do not bias correct EURO-CORDEX *tasmax* and *tasmin* here as we are only interested in their UHI trends, which are unaffected by removing the mean bias.

f. Emergence of temperature and UHI signals

To find year of emergence of temperature or UHI signals in UKCP18-regional, we use the most recent period, 2008–2018, as reference and construct a sample of 132 temperature or UHI intensity values (12 ensemble members $\times$ 11 years). We then move the analysis period forward by one year at a time, comparing the new sample of temperatures or UHI intensities to the reference sample using the Kolmogorov-Smirnov test (K-S test), akin to Mahlstein et al. (2012) and King et al. (2015)'s approach to estimating the time of emergence of local warming signals and climate extremes. The advantage of the K-S test is that it is sensitive to differences in both the location and shape of two samples. We compare the new sample of each subsequent period (up until 2069–2079) to that of the reference period in the same way and record all resulting p values. The middle year of the period in which the p value drops and remains below 0.05 is taken as year of emergence.

We also express emergence of temperature and UHI intensity signals in terms of the amount of global mean warming since 2008–2018 in the global simulations of UKCP18 (UKCP18-global), at the time when the temperature and UHI values become statistically significantly different from the 2008–2018 values at the 5% significance level. In other words, we find the amount of global

mean warming since 2008–2018 in the year of emergence and refer to it as "global mean warming of emergence". We choose 2008–2018 as reference because it is the period closest in time to the present that would have been validated against observations by the UK Met Office. Using the ensemble average of UKCP18-global (60 km) monthly mean temperature simulations, we find the amount of global mean warming since 2008–2018 for each period between 2008–2018 and 2069–2079. Global mean warming of emergence is the amount of global mean warming between 2008–2018 and the period of emergence (when p value drops and remains below 0.05).

To put global mean warming of emergence into the context of the Paris Agreement, we estimate the amount of global mean warming between the pre-industrial period (1850–1900) and 2008–2018 using the observational dataset HadCRUT4-CW (Cowtan and Way 2014). This dataset is based on Hadley Centre-Climatic Research Unit Version 4 (HadCRUT4) (Morice et al. 2012), but with missing values in HadCRUT4 filled by kriging (Cowtan and Way 2014). HadCRUT4-CW is more consistent with the UKCP18-global temperature simulations than HadCRUT4 (Murphy et al. 2018). We use HadCRUT4-CW to estimate global mean warming between pre-industrial times and the most recent decade because UKCP18-global does not cover the pre-industrial period. We find a global mean warming of 0.97°C between 1850–1900 and 2008–2018 from HadCRUT4-CW. This value is within the range of 0.8–1.2°C reported in the Special Report on Global Warming of 1.5°C produced by the Intergovernmental Panel on Climate Change (Intergovernmental Panel on Climate Change 2018). Adding 0.97°C to global mean warming of emergence allows us to compare our emergence results to the temperature thresholds of 1.5, 2 and 3°C above pre-industrial levels in Sections 3c and 3d.

3. Results

a. Projected urban and rural temperature trends

Figure 2 shows that both summer daytime and night-time temperatures over both urban and rural areas in UKCP18-regional are projected to increase with time in all studied cities in the period 1981–2079. This is expected from the increasing radiative forcing in RCP8.5. UKCP18-regional simulates larger upward trends in daytime than night-time temperature for both urban and rural areas.

Depending on the location, the warming rates of ensemble-mean rural daytime temperature range from 0.62 to 0.81°C per decade, whereas that of urban daytime temperature range from 0.57 to 0.78°C per decade (red dots in Figure 2). All these positive ensemble-mean daytime temperature trends are statistically significant at the 5% level. For all cities except Sheffield, a unit increase in rural daytime temperature is associated with a smaller increase in urban daytime temperature. These differential warming rates mean that daytime UHI intensity is expected to decrease with time in all studied cities but Sheffield (Figure 3 and top panel of Figure 4). The trends in UHI intensity will be explored in detail in the following section.

On the contrary, for every unit increase in ensemble-mean rural night-time temperature, there is a larger increase in urban night-time temperature (blue dots in Figure 2). This is true for all cities: the warming rates of rural night-time temperature range from 0.45 to 0.51°C per decade, whereas that of urban night-time temperature range from 0.48 to 0.55°C per decade. All these night-time warming trends are also statistically significant at the 5% level. However, higher night-time warming rates in urban areas than rural areas mean that ensemble-mean upward trends in night-time UHI intensity are expected in all cities in the period 1981–2079 (Figure 3 and top panel of Figure 4).

b. Projected UHI intensity trends

Figure 3 shows the time evolution of summer daytime and night-time UHI intensities in the cities between 1981 and 2079. These are UHI intensities calculated from bias-corrected UKCP18-regional temperatures (see Section 2e). The thin lines indicate simulations from individual UKCP18-regional ensemble members, whereas the thick lines indicate the ensemble means. Some cities (e.g. Newcastle) show a larger ensemble spread in simulated UHI intensity than other cities (e.g. Sheffield). These differences are not related to the differences in city size, average UHI intensity or warming level across the cities (not shown), and their causes will require research beyond this study.

For 7 of the cities (excluding Manchester, Sheffield and Bristol), UKCP18-regional simulates higher summer night-time than daytime UHI intensity in all years. This is consistent with the diurnal cycle of urban/rural temperature contrast reported in the literature (see Section 1). It is the result of larger urban thermal inertia that maintains a positive sensible heat flux and higher urban than rural air temperature at night.

While ensemble-mean summer night-time UHI intensities remain positive for all cities in almost all years, the ensemble-mean daytime UHI intensities for Birmingham, Leeds and Nottingham are consistently below 0°C during the 1981–2079 period (Figure 3). The ensemble-mean daytime UHI intensity is projected to drop below 0°C in Liverpool and Southampton in the second half of the simulation period too. This means summer urban cool islands exist in these cities during the day and they will strengthen in the 21st century, according to the UKCP18-regional simulations. These summer daytime urban cool islands are likely to be the result of a phase delay in the increase in upward sensible heat flux in the urban areas during the day because of their large thermal inertia (Bohnenstengel et al. 2011). We discuss urban cool islands around the world in Section 4.

By 2080, London's ensemble-mean summer night-time UHI intensity is projected to increase to 2.1°C, whereas its daytime UHI intensity is projected to decrease slightly to 0.8°C (Figure 3). An increase in ensemble-mean summer night-time UHI intensity is found for all cities, but at various rates (Figure 4 top panel). The four largest cities (London, Manchester, Birmingham and Leeds) show larger upward night-time UHI intensity trends (at 0.03–0.05°C per decade) than the rest of the cities. This suggests that future changes in night-time UHI intensity are related to the degree of urbanisation, even though urban fractions do not evolve with time in the simulations. Note that individual ensemble members of UKCP18-regional (crosses in Figure 4) do not agree on the sign of trend for Newcastle.

Conversely, the ensemble-mean summer daytime UHI intensity trends are downward in all cities except Sheffield (Figure 4 top panel). Manchester, Liverpool, Birmingham and Newcastle are projected to experience the largest mean downward trends at -0.04 to -0.05°C per decade. These downward trends may be linked to projected reductions in summer soil moisture in the UKCP18 simulations in the 21st century (Murphy et al. 2018). As soil moisture reduces, cooling through evapotranspiration in rural areas becomes less effective, reducing the urban/rural contrast in near-surface air temperature during the day, when most evapotranspiration occurs. The UKCP18-regional ensemble members do not agree on the sign of daytime UHI intensity trend in London, Nottingham and Sheffield, indicating less confidence in the overall trend for daytime than night-time UHI intensity in England.

Considering the three consecutive warmest days each year instead of the whole summer season amplifies the 1981–2079 ensemble-mean upward night-time UHI intensity trend and downward daytime UHI intensity trend in most cities (Figure 4 bottom panel). The most pronounced example for night-time UHI intensity trend amplification is Birmingham, which is projected to experience a 0.07°C per decade increase in night-time UHI intensity on its annual warmest days, compared

to a 0.04°C per decade increase over summers. For daytime UHI intensities, London would experience a -0.08°C per decade decrease in urban temperatures relative to rural temperatures on its annual warmest days, compared to a -0.004°C per decade decrease in daytime UHI intensity over summers. The sign of ensemble-mean trend changes from positive to negative for night-time UHI intensity in Sheffield and Bristol, and for daytime UHI intensity in Sheffield. The ensemble spread is generally larger on annual warmest days than over summers due to increased variability, leading to more ensemble disagreements on the sign of trends.

c. Emergence of temperature signals

We examine whether the upward trends in summer daytime and night-time temperatures over the studied urban and rural areas (Figure 2) would emerge from climate variability in UKCP18-regional in this section. Figure 5 shows the global mean warming of emergence of summer urban (filled triangles) and rural (empty triangles), daytime (red) and night-time (blue) temperature signals in and surrounding the cities. The right y-axis of Figure 5 indicates the corresponding year of emergence based on the ensemble mean of UKCP18-global, expressed in the number of years after 2013 (the middle year of the reference period, 2008–2018). Recall that year of emergence is defined as the middle year of the future 11-year period during which the new temperature distribution is statistically significantly different from the reference (2008–2018) distribution at the 5% level (see Section 2f).

The distributions of summer urban and rural, daytime and night-time temperatures would be statistically significantly (at the 5% level) different from their respective 2008–2018 distributions when the globe becomes 0.2–0.27°C warmer than the 2008–2018 period. This means the positive temperature signals would all emerge below 1.25°C global warming above pre-industrial levels, below the 1.5°C Paris Agreement limit.

As shown by the right y-axis of Figure 5; all summer urban and rural, daytime and night-time temperature signals are expected to emerge from 2008–2018 variability earlier than or about 6 years after 2013, if the model is correct. This means around year 2019, the middle year of the 2014–2024 period, all these temperature signals would emerge in the UKCP18 simulations. At the time of writing (early 2020), this means there is a ∼50% chance that these positive daytime and night-time temperature signals have already emerged from 2008–2018 variability over the included urban and rural grid boxes. This also means that these warming signals are projected to emerge within half a decade if they have not already.

d. Emergence of UHI signals

We now investigate whether the differential trends in summer daytime and night-time UHI intensity would also emerge from 2008–2018 variability in the UKCP18 simulations. Figure 6 shows the global mean warming of emergence of summer daytime and night-time UHI signals in the cities, with indicators of the 1.5 and 2°C Paris Agreement targets, and the 3°C global warming above pre-industrial levels implied by current NDCs. It also shows the corresponding year of emergence for completion.

In all cities except Newcastle, the upward trend in summer night-time UHI intensity (upward blue triangles in Figure 6) would emerge from 2008–2018 variability when global mean warming goes above 0.8°C above the most recent (2008–2018) levels. At 0.8–0.9°C above the most recent levels, summer night-time UHI intensities in Birmingham and Leeds would become statistically significantly higher (at the 5% level) than their reference values. Five other cities (Bristol, Southampton, London, Manchester and Liverpool) would have their summer night-time UHI intensity signals emerge from variability ∼1– 2°C above the 2008–2018 levels; that is, 2–3°C above pre-industrial levels. In Nottingham and Sheffield, the positive summer night-time UHI intensity

signal would emerge at 2.9 and 3.2°C global warming above the 2008–2018 levels; that is, ∼4°C above pre-industrial levels.

At their respective global mean warming of emergences, the magnitudes of summer night-time UHI intensity in the cities (except Newcastle) are projected to be: (in ascending order of emergence) 0.6°C in Birmingham, 0.1°C in Leeds, 0.4°C in Bristol, 0.8°C in Southampton, 1.8°C in London, 1.4°C in Manchester, 1.5°C in Liverpool, 0.3°C in Nottingham, and 1°C in Sheffield.

Nine of the cities (excluding Sheffield) would have their summer daytime UHI intensity reductions emerge from 2008–2018 variability in the UKCP18-regional simulations (downward red triangles in Figure 6 indicate negative daytime UHI signals). In many of these places (except London and Nottingham), the daytime emergences happen at lower global warming levels than the corresponding night-time emergences. The global mean warming of emergences of the daytime UHI intensity signal in Manchester, Liverpool, Birmingham, Bristol and Southampton range between 0.2 and 0.5°C above the 2008–2018 levels. These are equivalent to warmings below 1.5°C above pre-industrial levels, i.e. the stricter Paris Agreement target. By 2 and 3°C global warming above pre-industrial levels; the downward trend in summer daytime UHI intensity in Leeds and Newcastle would also emerge.

At their respective global mean warming of emergences, the magnitudes of summer daytime UHI intensity in the cities (except Sheffield) are projected to be: (in ascending order of emergence) 1°C in Manchester, -0.05°C in Liverpool, -0.7°C in Birmingham, 0.6°C in Bristol, 0.3°C in Southampton, -0.9°C in Leeds, 0.9°C in Newcastle, -0.4°C in Nottingham, and 0.9°C in London. More than half of these cities would still be warmer than their rural surroundings during the day despite the projected emergent, downward trends in daytime UHI intensity.

With few exceptions, we find higher global mean warming of emergences of daytime and night-time UHI intensity signals on annual warmest days than in summer (not shown), even though most

of the trends are amplified on annual warmest days. We attribute this to increased intra-ensemble and inter-annual UHI intensity variabilities when considering only the three consecutive warmest days each year. Nevertheless, the emergent yet opposite trends in daytime and night-time UHI intensity found in this study provide a scientific basis for future urban planning in England.

4. Discussion

Assuming constant urbanisation in UKCP18-regional, we have found upward trends in bias-corrected, summer daytime and night-time temperatures over both urban and rural grid boxes in the 10 most populous built-up areas in England over the period 1981–2079. Despite their varying warming rates (Figure 2), all these temperature signals are projected to emerge from 2008–2018 variability below 1.25°C global mean warming above pre-industrial (1850–1900) levels. According to UKCP18-global, these emergences are expected to occur in 11-year periods centred on or before year 2019, suggesting that they may have already occurred (Figure 5).

Using a different reference period (1860–1910) and 23 climate model simulations, King et al. (2015) found the median time of emergence of summer highest maximum temperature to be between 2000 and 2020 over the UK, whereas that of summer lowest minimum temperature to be between 1980 and 2020. We are unable to compare our results with King et al. (2015)'s like-for-like due to a lack of pre-1980 UKCP18-regional data. Nevertheless, both our studies suggest that emergence of warming signals may have already occurred in at least part of the UK. This has important implications to UK's public health as elevated summer temperatures are known to increase heat stress, inhibit recovery from heat loads and disrupt sleep (Libert et al. 1988; Fischer and Schär 2010; Grize et al. 2005).

UKCP18-regional projects, on average, a 0.05°C per decade increase in summer night-time UHI intensity in London, from ∼1.6°C in the 1980s to 2.1°C by 2080 (Figures 3 and 4). Our 1980s

value is lower than the observed $\sim$2°C, which was estimated by Wilby (2003) through comparing 1961–1990 summer temperatures between an urban and a rural weather station in London. This suggests that our UHI estimates are conservative as a result of our two-grid approach to identifying urban and rural areas (Section 2d). However, our approach provides a new way for systematically estimating UHI intensities across the UK from gridded datasets, rather than individual weather stations that are prone to errors and uncertainty.

Using climate and statistical models, Wilby (2003) projected a 0.3°C increase in London's summer night-time UHI intensity between 1961–1990 and the 2080s, whereas Wilby (2008) projected a strengthening of summer night-time UHI intensity to $\sim$3 °C in London by the 2050s. By coupling an RCM to an urban surface scheme, however, Mccarthy et al. (2012) simulated an unaltered summer night-time UHI for London between 1971–1990 and 2041–2060. Our results are qualitatively consistent with the former two studies, given that a different future climate change scenario (RCP8.5) is used here.

In the daytime, we have found that summer urban cool islands exist and will strengthen with time in 5 included cities (Figure 3). Summer daytime urban cool islands have been observed in various parts of the world (Yang et al. 2017), including in mid-latitude European cities (Acero et al. 2013; Gonçalves et al. 2018), albeit less frequently than urban heat islands. In addition to a daytime sensible heat flux phase delay (Section 3b); urban cool islands around the world have been attributed to air pollution attenuating solar radiation (Memon et al. 2009), little anthropogenic heat from cars and homes (Yang et al. 2017), cool urban green spaces as a result of evapotranspiration and shading by trees (Gonçalves et al. 2018), sea breeze cooling of coastal cities (Suomi and Käyhkö 2012; Acero et al. 2013), differences between early morning urban and rural mixed layer depths (Theeuwes et al. 2015), and tall buildings shading the street level (Oke 1987; Erell and

Williamson 2007). However, tall buildings are not captured in UKCP18-regional's one-tile urban scheme (see Section 2b).

Mccarthy et al. (2012) simulated a 0.1°C decrease in summer daytime UHI intensity for London between 1971–1990 and 2041–2060. The UKCP18-regional ensemble mean also simulates a decrease in London's summer daytime UHI intensity over time, although individual ensemble members disagree on the sign of change (Figure 4). Previous studies on UHI projection in the UK mainly focused on the night-time intensity in London, making comparison of the rest of our projections with the literature impossible. By filling this gap in the literature, our study provides the basis for future comparisons when more research on daytime UHI intensity changes in smaller UK cities become available.

For other parts of the world, various changes in UHI intensity have been projected in previous studies, depending on the region, season and climate change scenario (Oleson et al. 2011; Oleson 2012; Argüeso et al. 2014; Lauwaet et al. 2015; Chapman et al. 2017). In Europe, a decrease in summer daytime UHI intensity (Hamdi et al. 2014, 2015), and an unaltered or a decrease in summer night-time UHI intensity (Hamdi et al. 2014; Lauwaet et al. 2016) were projected for Brussels; a decrease in both summer daytime (Hamdi et al. 2015) and night-time UHI intensities (Lemonsu et al. 2013) was projected for Paris; whereas an increase in average summer UHI intensity was projected for Berlin (Grossman-Clarke et al. 2017). It should be noted, however, that UHIs can also occur in winter; although they are generally less pronounced than summer UHIs in the UK and other mid-latitude cities (Kershaw et al. 2010). This is because absorption of solar radiation by buildings dominates the formation of UHIs in summer in these cities (Kershaw et al. 2010). For Arctic climates, more pronounced winter UHI increases were observed than summer UHI increases (e.g. Magee et al. 1999), but this is beyond the scope of this study.

As evidenced by the examples for London and Brussels above, contrasting UHI projections can be found for the same UHI metric and season in the literature as a result of different modelling methods. Our focus in this study has been on the new UKCP18-regional dataset because it is the gold standard for UK climate simulations. It was specifically designed for research like this, with enough ensemble members to show confidence in the results. Figure A4 shows that selected EURO-CORDEX models (see Section 2c) simulate a range of summer UHI intensity responses in the included cities under RCP8.5. For daytime UHI, WRF381P and REMO2009 simulate smaller, and in some cases opposite, trends than UKCP18-regional and HadREM3-GA7-05 (EURO-CORDEX version). For night-time UHI, there is little agreement between EURO-CORDEX and UKCP18-regional. Therefore, the main results of this study — a projected decrease in summer daytime and a projected increase in summer night-time UHI intensity in major English cities — are specific to the UKCP18-regional configuration, which we believe is best suited for this analysis.

Based on UKCP18-regional, the downward summer daytime UHI intensity signals in UKCP18-regional would emerge from 2008–2018 variability in 5 included cities before global mean temperature reaches 1.5°C above pre-industrial levels (Figure 6). We stress that this does not mean climate change will be beneficial to increasing thermal comfort in urban areas, because both urban and rural temperatures are expected to rise significantly in the 21st century (Figure 2). A reduction in daytime UHI intensity is simply the outcome of different rates of warming between urban and rural areas.

Conversely, the upward night-time UHI intensity signals would emerge in 7 cities below 3°C global mean warming above pre-industrial levels, further strengthening the contrasts between rising urban and rural temperatures around these cities. These emergent changes might alter

mesoscale atmospheric circulations and in turn the spatial and diurnal distributions of air pollutants (see Section 1), although research is needed to test this hypothesis.

This study has made use of the newest generation of UKCP to estimate future changes in, and potential emergences of, summer temperatures and UHI intensities in England. While UKCP18-regional is state-of-the-art in many ways (Murphy et al. 2018), this urban heat study comes with a few limitations. As shown above, our main results are specific to the UKCP18-regional configuration. Having focused on UKCP18-regional rather than EURO-CORDEX, the latter of which was not solely designed for UK climate projections, we have not investigated the reasons behind the differences in UHI intensity trends between the climate models.

Secondly, UKCP18-regional does not include time-varying urban land use (see Section 2b). Our urban temperature and UHI emergence estimates are therefore based on present-day urbanisation and projected climate warming. Thirdly, the 12 km resolution of UKCP18-regional is just fine enough to revolve the Bristol BUA (Table 1). This may have led to an underestimation of UHI intensities in the smaller cities.

Moreover, sub-daily air temperature, cloud cover and wind outputs are not available from UKCP18-regional at the time of writing. By using the urban/rural differences in daily maximum and minimum temperatures as proxies for daytime and night-time UHI intensities, we have not accounted for the fact that daily maximum and minimum temperatures often occur at different times in urban and rural areas due to a phase shift in the surface energy balance (see Section 1). Without sub-daily cloud cover and wind data, or any soil moisture data at the global or regional scale, we have only been able to qualitatively discuss the potential reasons for decreasing summer daytime UHI intensities and the potential impacts of future UHI intensity changes on air pollutant concentrations.

Future research is recommended to investigate the drivers of the differences in UHI intensity trends between UKCP18-regional and EURO-CORDEX simulations. To understand how future urbanisation and climate change will affect urban and rural temperatures and the UHI effect, future work could expand this work by incorporating land use as well as climate projections. Earlier this year the UK Met Office released UKCP18-local, a set of 2.2 km projections that resolve small-scale phenomena including atmospheric convection (Kendon et al. 2019). The convection-permitting model uses a two-tile urban scheme that represents roofs and street canyon facets (Porson et al. 2010), instead of the one-tile scheme used in UKCP18-regional (Section 2b). Sub-daily climate variable outputs are also becoming available for time slices spanning 1981–2000, 2021–2040 and 2061–2080 as this paper is being written (Kendon et al. 2019). This sub-daily dataset will be very useful for understanding the processes that drive the differential changes between daytime and night-time UHIs found in this study. Using UKCP18-local to further explore potential changes in the UHI effect, the drivers of these changes and their impacts should be a priority of future work.

5. Conclusions

Rising urban and rural temperatures could increase human heat stress. Changes in UHI intensities could alter local atmospheric circulations and, in turn, distributions of air pollutants. Using UKCP18-regional, the 12 km simulations from the newest generation of the UK climate projections, we quantify trends in summer daytime and night-time temperatures in urban and rural areas, as well as the UHI intensities in the 10 most populous built-up areas in England in the period 1981–2079. We find an increasing trend in both urban and rural daytime and night-time temperatures in the RCP8.5 scenario. There is a $\sim$50% chance that positive temperature signals from all 10 cities have already emerged from 2008–2018 variability.

Projected differential warming rates between summer urban and rural temperatures mean that summer daytime UHI intensity would decrease by -0.004 to -0.05°C per decade in nine of the cities, whereas summer night-time UHI intensity would increase by 0.01 to 0.05°C per decade in all cities. The negative daytime UHI signals would emerge in Manchester, Liverpool, Birmingham, Bristol and Southampton before global mean warming reaches 1.5°C above pre-industrial levels, and in Leeds between 1.5 and 2°C global warming. Conversely, the increasing night-time UHI signals would emerge from 2008–2018 variability in Birmingham and Leeds when global mean warming is between 1.5 and 2°C above pre-industrial levels. These results provide important information for future municipal adaptation and urban planning in the UK, in the context of internationally recognised temperature thresholds. Since our emergence results are based on present-day urbanisation and projected climate warming in UKCP18-regional, increasing urbanisation would exacerbate the projected changes in urban temperatures and UHI intensities, potentially leading to earlier emergence.

Acknowledgments. We thank the UKCP18 team at the UK Met Office for making the data available. Data used in this manuscript are licensed under the Open Government Licence v3.0. We thank Lizzie Kendon and Simon Tucker for providing the land surface data of UKCP18. HadUK-Grid data can be accessed at `http://catalogue.ceda.ac.uk/uuid/4dc8450d889a491ebb20e724debe2dfb`; UKCP18-regional data on a 12 km grid over the UK can be accessed at `https://catalogue.ceda.ac.uk/uuid/589211abeb844070a95d061c8cc7f604`; whereas EURO-CORDEX data can be accessed at `https://www.euro-cordex.net/060378/index.php.en`. Y. T. E. Lo was supported by NERC Research Grant NE/R009554/1. D. M. Mitchell was supported by NERC Independent Research Fellowship NE/N014057/1. The authors declare that they have no conflict of interest.

References

Acero, J. A., J. Arrizabalaga, S. Kupski, and L. Katzschner, 2013: Urban heat island in a coastal urban area in northern Spain. *Theoretical and Applied Climatology*, **113 (1-2)**, 137–154, doi: 10.1007/s00704-012-0774-z.

Agarwal, M., and A. Tandon, 2010: Modeling of the urban heat island in the form of mesoscale wind and of its effect on air pollution dispersal. *Applied Mathematical Modelling*, **34 (9)**, 2520–2530, doi:10.1016/j.apm.2009.11.016, URL http://dx.doi.org/10.1016/j.apm.2009.11.016.

Allen, L., F. Lindberg, and C. S. B. Grimmond, 2011: Global to city scale urban anthropogenic heat flux: Model and variability. *International Journal of Climatology*, **31 (13)**, 1990–2005, doi:10.1002/joc.2210.

Argüeso, D., J. P. Evans, L. Fita, and K. J. Bormann, 2014: Temperature response to future urbanization and climate change. *Climate Dynamics*, **42 (7-8)**, 2183–2199, doi:10.1007/s00382-013-1789-6.

Basara, J. B., H. G. Basara, B. G. Illston, and K. C. Crawford, 2010: The Impact of the Urban Heat Island during an Intense Heat Wave in Oklahoma City. *Advances in Meteorology*, **2010**, 1–10, doi:10.1155/2010/230365.

Best, M. J., 2005: Representing urban areas within operational numerical weather prediction models. *Boundary-Layer Meteorology*, **114 (1)**, 91–109, doi:10.1007/s10546-004-4834-5.

Best, M. J., and Coauthors, 2011: The Joint UK Land Environment Simulator (JULES), model description – Part 1: Energy and water fluxes. *Geoscientific Model Development*, **4 (3)**, 677–699, doi:10.5194/gmd-4-677-2011.

Bodas-Salcedo, A., J. P. Mulcahy, T. Andrews, K. D. Williams, M. A. Ringer, P. R. Field, and G. S. Elsaesser, 2019: Strong Dependence of Atmospheric Feedbacks on Mixed-Phase Microphysics and Aerosol-Cloud Interactions in HadGEM3. *Journal of Advances in Modeling Earth Systems*, **11**, 1735–1758, doi:10.1029/2019MS001688.

Bohnenstengel, S. I., S. Evans, P. A. Clark, and S. E. Belcher, 2011: Simulations of the London urban heat island. *Quarterly Journal of the Royal Meteorological Society*, **137 (659)**, 1625–1640, doi:10.1002/qj.855.

Bohnenstengel, S. I., I. Hamilton, M. Davies, and S. E. Belcher, 2014: Impact of anthropogenic heat emissions on London's temperatures. *Quarterly Journal of the Royal Meteorological Society*, **140 (679)**, 687–698, doi:10.1002/qj.2144.

Chapman, S., J. E. Watson, A. Salazar, M. Thatcher, and C. A. McAlpine, 2017: The impact of urbanization and climate change on urban temperatures: a systematic review. *Landscape Ecology*, **32 (10)**, 1921–1935, doi:10.1007/s10980-017-0561-4.

Cowtan, K., and R. G. Way, 2014: Coverage bias in the HadCRUT4 temperature series and its impact on recent temperature trends. *Quarterly Journal of the Royal Meteorological Society*, **140 (683)**, 1935–1944, doi:10.1002/qj.2297.

Cui, Y. Y., and B. De Foy, 2012: Seasonal variations of the urban heat island at the surface and the near-surface and reductions due to urban vegetation in Mexico City. *Journal of Applied Meteorology and Climatology*, **51 (5)**, 855–868, doi:10.1175/JAMC-D-11-0104.1.

Dufresne, J. L., and Coauthors, 2013: Climate change projections using the IPSL-CM5 Earth System Model: From CMIP3 to CMIP5. *Climate Dynamics*, **40 (9-10)**, 2123–2165, doi:10.1007/s00382-012-1636-1.

Erell, E., and T. Williamson, 2007: Intra-urban differences in canopy layer air temperature at a mid-latitude city. *International Journal of Climatology*, **27**, 1243–1255, doi:10.1002/joc.1469.

Fallmann, J., R. Forkel, and S. Emeis, 2016: Secondary effects of urban heat island mitigation measures on air quality. *Atmospheric Environment*, **125**, 199–211, doi:10.1016/j.atmosenv.2015.10.094.

Fenner, D., A. Holtmann, F. Meier, I. Langer, and D. Scherer, 2019: Contrasting changes of urban heat island intensity during hot weather episodes. *Environmental Research Letters*, **14**, doi:10.1088/1748-9326/ab506b, URL http://iopscience.iop.org/article/10.1088/1748-9326/ab506b.

Fischer, E. M., K. W. Oleson, and D. M. Lawrence, 2012: Contrasting urban and rural heat stress responses to climate change. *Geophysical Research Letters*, **39 (3)**, 1–8, doi:10.1029/2011GL050576.

Fischer, E. M., and C. Schär, 2010: Consistent geographical patterns of changes in high-impact European heatwaves. *Nature Geoscience*, **3 (6)**, 398–403, doi:10.1038/ngeo866.

Giorgetta, M. A., and Coauthors, 2013: Climate and carbon cycle changes from 1850 to 2100 in MPI-ESM simulations for the Coupled Model Intercomparison Project phase 5. *Journal of Advances in Modeling Earth Systems*, **5 (3)**, 572–597, doi:10.1002/jame.20038.

Gonçalves, A., G. Ornellas, A. C. Ribeiro, F. Maia, A. Rocha, and M. Feliciano, 2018: Urban cold and Heat Island in the City of Bragança (Portugal). *Climate*, **6 (3)**, 1–14, doi:10.3390/cli6030070.

Grize, L., A. Huss, O. Thommen, C. Schindler, and C. Braun-Fahrländer, 2005: Heat wave 2003 and mortality in Switzerland. *Swiss Medical Weekly*, **135 (13-14)**, 200–205.

Grossman-Clarke, S., S. Schubert, and D. Fenner, 2017: Urban effects on summertime air temperature in Germany under climate change. *International Journal of Climatology*, **37 (2)**, 905–917, doi:10.1002/joc.4748.

Hamdi, R., O. Giot, R. De Troch, A. Deckmyn, and P. Termonia, 2015: Future climate of Brussels and Paris for the 2050s under the A1B scenario. *Urban Climate*, **12**, 160–182, doi:10.1016/j.uclim.2015.03.003, URL http://dx.doi.org/10.1016/j.uclim.2015.03.003.

Hamdi, R., H. Van de Vyver, R. De Troch, and P. Termonia, 2014: Assessment of three dynamical urban climate downscaling methods: Brussels's future urban heat island under an A1B emission scenario. *International Journal of Climatology*, **34 (4)**, 978–999, doi:10.1002/joc.3734.

Heaviside, C., X. M. Cai, and S. Vardoulakis, 2015: The effects of horizontal advection on the urban heat island in Birmingham and the West Midlands, United Kingdom during a heatwave. *Quarterly Journal of the Royal Meteorological Society*, **141 (689)**, 1429–1441, doi:10.1002/qj.2452.

Heaviside, C., S. Vardoulakis, and X.-M. Cai, 2016: Attribution of mortality to the urban heat island during heatwaves in the West Midlands, UK. *Environmental Health*, **15 (27)**, 49–59, doi:10.1186/s12940-016-0100-9.

Hollis, D., M. McCarthy, M. Kendon, T. Legg, and I. Simpson, 2019: HadUK-Grid—A new UK dataset of gridded climate observations. *Geoscience Data Journal*, **6 (2)**, 151–159, doi:10.1002/gdj3.78.

Intergovernmental Panel on Climate Change, 2018: Summary for Policymakers. *Special Report on Global Warming of 1.5 °C*, 1–33, URL http://report.ipcc.ch/sr15/pdf/sr15{_}spm{_}final.pdf.

Jacob, D., and Coauthors, 2012: Assessing the transferability of the regional climate model REMO to different coordinated regional climate downscaling experiment (CORDEX) regions. *Atmosphere*, **3 (1)**, 181–199, doi:10.3390/atmos3010181.

Jacob, D., and Coauthors, 2014: EURO-CORDEX: New high-resolution climate change projections for European impact research. *Regional Environmental Change*, **14 (2)**, 563–578, doi:10.1007/s10113-013-0499-2.

Jones, C. D., and Coauthors, 2011: The HadGEM2-ES implementation of CMIP5 centennial simulations. *Geoscientific Model Development*, **4 (3)**, 543–570, doi:10.5194/gmd-4-543-2011.

Kendon, E., and Coauthors, 2019: UKCP Convection-permitting model projections : Science report. Tech. Rep. 1, UK Met Office, 1–153 pp.

Kershaw, T., M. Sanderson, D. Coley, and M. Eames, 2010: Estimation of the urban heat island for UK climate change projections. *Building Services Engineering Research and Technology*, **31 (3)**, 251–263, doi:10.1177/0143624410365033.

King, A. D., and Coauthors, 2015: The timing of anthropogenic emergence in simulated climate extremes. *Environmental Research Letters*, **10 (9)**, doi:10.1088/1748-9326/10/9/094015.

Lauwaet, D., K. De Ridder, S. Saeed, E. Brisson, F. Chatterjee, N. P. van Lipzig, B. Maiheu, and H. Hooyberghs, 2016: Assessing the current and future urban heat island of Brussels. *Urban Climate*, **15**, 1–15, doi:10.1016/j.uclim.2015.11.008, URL http://dx.doi.org/10.1016/j.uclim.2015.11.008.

Lauwaet, D., H. Hooyberghs, B. Maiheu, W. Lefebvre, G. Driesen, S. Van Looy, and K. De Ridder, 2015: Detailed urban heat island projections for cities worldwide: Dynamical downscaling CMIP5 global climate models. *Climate*, **3 (2)**, 391–415, doi:10.3390/cli3020391.

Lee, D. O., 1979: The influence of atmospheric stability and the urban heat island on urban-rural wind speed differences. *Atmospheric Environment (1967)*, **13 (8)**, 1175–1180, doi:10.1016/0004-6981(79)90042-8.

Lemonsu, A., R. Kounkou-Arnaud, J. Desplat, J. L. Salagnac, and V. Masson, 2013: Evolution of the Parisian urban climate under a global changing climate. *Climatic Change*, **116 (3-4)**, 679–692, doi:10.1007/s10584-012-0521-6.

Levermore, G., J. Parkinson, K. Lee, P. Laycock, and S. Lindley, 2018: The increasing trend of the urban heat island intensity. *Urban Climate*, **24**, 360–368, doi:10.1016/j.uclim.2017.02.004.

Libert, J. P., J. Di Nisi, H. Fukuda, A. Muzet, J. Ehrhart, and C. Amoros, 1988: Effect of Continuous Heat Exposure on Sleep Stages in Humans. *Sleep*, **11 (2)**, 195–209.

Lo, Y. T. E., and Coauthors, 2019: Increasing mitigation ambition to meet the Paris Agreement ' s temperature goal avoids substantial heat-related mortality in U . S . cities. *Science Advances*, **5 (6)**, eaau4373, doi:10.1126/sciadv.aau4373.

Magee, N., J. Curtis, and G. Wendler, 1999: The urban heat island effect at Fairbanks, Alaska. *Theoretical and Applied Climatology*, **64 (1-2)**, 39–47, doi:10.1007/s007040050109.

Mahlstein, I., G. Hegerl, and S. Solomon, 2012: Emerging local warming signals in observational data. *Geophysical Research Letters*, **39 (21)**, 1–5, doi:10.1029/2012GL053952.

Mccarthy, M. P., C. Harpham, C. M. Goodess, and P. D. Jones, 2012: Simulating climate change in UK cities using a regional climate model, HadRM3. *International Journal of Climatology*, **32 (12)**, 1875–1888, doi:10.1002/joc.2402.

742 Memon, R. A., D. Y. Leung, and C. H. Liu, 2009: An investigation of urban heat island intensity
743 (UHII) as an indicator of urban heating. *Atmospheric Research*, **94 (3)**, 491–500, doi:10.1016/j.
744 atmosres.2009.07.006.

745 Morice, C. P., J. J. Kennedy, N. A. Rayner, and P. D. Jones, 2012: Quantifying uncertainties
746 in global and regional temperature change using an ensemble of observational estimates: The
747 HadCRUT4 data set. *Journal of Geophysical Research Atmospheres*, **117 (8)**, 1–22, doi:10.
748 1029/2011JD017187.

749 Murphy, J., and Coauthors, 2009: UK Climate Projections Science Report: Climate
750 change projections. Tech. rep., Met Office Hadley Centre, Exeter, 1–190 pp. doi:10.1787/
751 9789264086876-5-en.

752 Murphy, J. M., and Coauthors, 2018: UKCP18 Land Projections: Science Report. Tech. rep.,
753 1–191 pp.

754 Office for National Statistics, 2013: 2011 Built-up Areas - Methodology and Guidance. Tech. rep.,
755 Office for National Statistics, 1–15 pp.

756 Oke, T. R., 1987: *Boundary Layer Climates*. 2nd ed., Taylor & Francis.

757 Oleson, K., 2012: Contrasts between Urban and rural climate in CCSM4 CMIP5 climate change
758 scenarios. *Journal of Climate*, **25 (5)**, 1390–1412, doi:10.1175/JCLI-D-11-00098.1.

759 Oleson, K. W., G. B. Bonan, J. Feddema, and T. Jackson, 2011: An examination of urban heat
760 island characteristics in a global climate model. *International Journal of Climatology*, **31 (12)**,
761 1848–1865, doi:10.1002/joc.2201.

762 Porson, A., P. A. Clark, I. N. Harman, M. J. Best, and S. E. Belcher, 2010: Implementation of a
763 new urban energy budget scheme in the MetUM. Part I: Description and idealized simulations.

Quarterly Journal of the Royal Meteorological Society, **136 (651)**, 1514–1529, doi:10.1002/qj.668.

Rainham, D. G., and K. E. Smoyer-Tomic, 2003: The role of air pollution in the relationship between a heat stress index and human mortality in Toronto. *Environmental Research*, **93 (1)**, 9–19, doi:10.1016/S0013-9351(03)00060-4.

Rogelj, J., and Coauthors, 2016: Paris Agreement climate proposals need a boost to keep warming well below 2 °C. *Nature*, **534 (7609)**, 631–639, doi:10.1038/nature18307.

Sachindra, D. A., A. W. Ng, S. Muthukumaran, and B. J. Perera, 2016: Impact of climate change on urban heat island effect and extreme temperatures: A case-study. *Quarterly Journal of the Royal Meteorological Society*, **142 (694)**, 172–186, doi:10.1002/qj.2642.

Sarrat, C., A. Lemonsu, V. Masson, and D. Guedalia, 2006: Impact of urban heat island on regional atmospheric pollution. *Atmospheric Environment*, **40 (10)**, 1743–1758, doi:10.1016/j.atmosenv.2005.11.037.

Schlünzen, K. H., and S. I. Bohnenstengel, 2016: *Socio-economic Impacts—Urban Climate*, 417–429. Springer International Publishing, Cham, doi:10.1007/978-3-319-39745-0_15, URL https://doi.org/10.1007/978-3-319-39745-0_15.

Smith, C. L., A. Webb, G. J. Levermore, S. J. Lindley, and K. Beswick, 2011: Fine-scale spatial temperature patterns across a UK conurbation. *Climatic Change*, **109 (3-4)**, 269–286, doi:10.1007/s10584-011-0021-0.

Suomi, J., and J. Käyhkö, 2012: The impact of environmental factors on urban temperature variability in the coastal city of Turku, SW Finland. *International Journal of Climatology*, **32 (3)**, 451–463, doi:10.1002/joc.2277.

Tan, J., and Coauthors, 2010: The urban heat island and its impact on heat waves and human health in Shanghai. *International Journal of Biometeorology*, **54 (1)**, 75–84, doi:10.1007/s00484-009-0256-x.

Taylor, K. E., R. J. Stouffer, and G. A. Meehl, 2012: An overview of CMIP5 and the experiment design. *Bulletin of the American Meteorological Society*, **93 (4)**, 485–498, doi:10.1175/BAMS-D-11-00094.1.

Theeuwes, N. E., G. J. Steeneveld, R. J. Ronda, M. W. Rotach, and A. A. Holtslag, 2015: Cool city mornings by urban heat. *Environmental Research Letters*, **10 (11)**, doi:10.1088/1748-9326/10/11/114022.

UK Met Office, 2019: Heatwave. URL https://www.metoffice.gov.uk/weather/learn-about/weather/types-of-weather/temperature/heatwave.

UNFCCC, 2015: Adoption of the Paris Agreement. Tech. rep., 1–32 pp. doi:FCCC/CP/2015/L.9/Rev.1.

United Nations, 2018: 68% of the world population projected to live in urban areas by 2050, says UN. URL https://www.un.org/development/desa/en/news/population/2018-revision-of-world-urbanization-prospects.html.

United Nations DESA/Population Division, 2018: World Urbanization Prospects 2018 - Country Profiles. URL https://population.un.org/wup/Country-Profiles/.

Vicedo-Cabrera, A. M., and Coauthors, 2018: Temperature-mortality impacts under and beyond Paris Agreement climate change scenarios. *Climate Change Letters*, **150**, 391–402, doi:10.1007/s10584-018-2274-3.

Vukovich, F. M., W. J. King, J. W. Dunn III, and J. J. B. Worth, 1979: Observations and Simulations of the Diurnal Variation of the Urban Heat Island Circulation and Associated Variations of the Ozone Distribution: A Case Study. 836–854 pp.

Wilby, R. L., 2003: Past and projected trends in London's urban heat island. *Weather*, **58 (7)**, 251–260, doi:10.1256/wea.183.02.

Wilby, R. L., 2008: Constructing climate change scenarios of urban heat island intensity and air quality. *Environment and Planning B: Planning and Design*, **35 (5)**, 902–919, doi:10.1068/b33066t.

Yamamoto, Y., 2006: Measures to Mitigate Urban Heat Islands. *Quaterly Review*, **18**, 65–83.

Yang, X., Y. Li, Z. Luo, and P. W. Chan, 2017: The urban cool island phenomenon in a high-rise high-density city and its mechanisms. *International Journal of Climatology*, **37 (2)**, 890–904, doi:10.1002/joc.4747.

Zhang, N., X. Wang, and Z. Peng, 2014: Large-Eddy Simulation of Mesoscale Circulations Forced by Inhomogeneous Urban Heat Island. *Boundary-Layer Meteorology*, **151 (1)**, 179–194, doi:10.1007/s10546-013-9879-x.

APPENDIX

LIST OF TABLES

824 TABLE 1. The 10 most populous built-up areas (BUAs) and the cities therein included in this study, listed in
825 descending order of their 2016 population estimates (not shown) (Office for National Statistics 2013). The right
826 columns show the urban fractions in urban and rural grid boxes in each area.

BUA	City	BUA size (km^2)	Highest urban fractions	Lowest urban fractions
Greater London	London	1737.9	0.88, 0.92	0.06, 0.07
Greater Manchester	Manchester	630.3	0.48, 0.59	0.04, 0.04
West Midlands	Birmingham	598.9	0.64, 0.64	0.02, 0.02
West Yorkshire	Leeds	487.8	0.42, 0.48	0.01, 0.01
Liverpool	Liverpool	199.6	0.36, 0.41	0.01, 0.03
South Hampshire	Southampton	192.0	0.24, 0.27	0.00, 0.00
Tyneside	Newcastle	180.5	0.33, 0.43	0.00, 0.00
Nottingham	Nottingham	176.4	0.23, 0.27	0.00, 0.00
Sheffield	Sheffield	167.5	0.26, 0.27	0.00, 0.00
Bristol	Bristol	144.4	0.16, 0.16	0.00, 0.00

827 **LIST OF FIGURES**

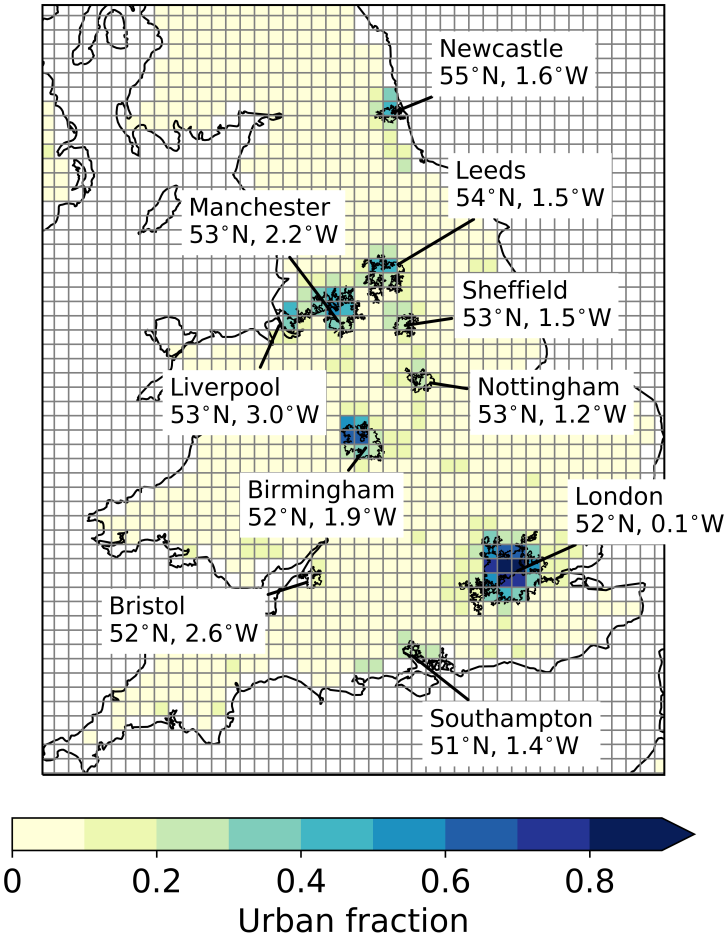

828 FIG. 1. Urban fraction in the 12 km grids of the UKCP18-regional simulations overlaid with the boundaries of
829 the 10 most populous urban built-up areas in England, according to data from the Office for National Statistics.
830 The urban fractions do not change between 1980 and 2080. The latitude and longitude of individual cities are
831 indicated. This map is shown in the the Ordnance Survey's British National Grid.

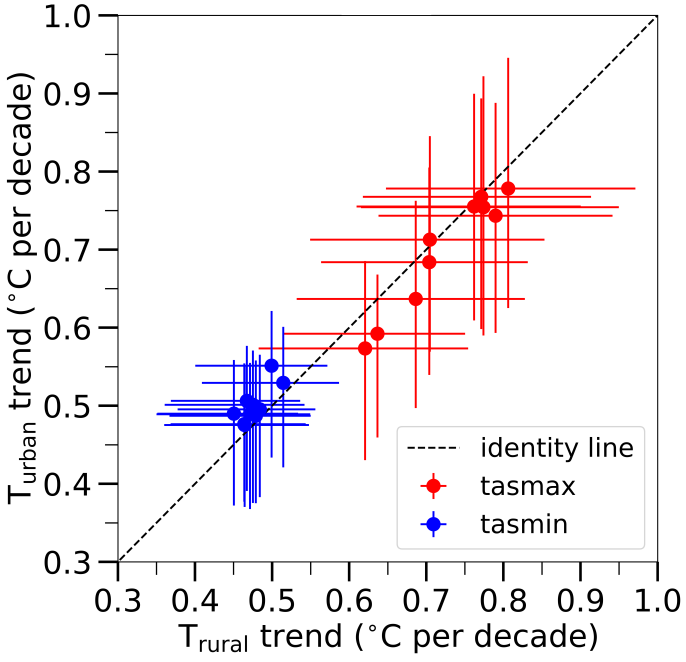

832 FIG. 2. Comparison of trends of urban and rural temperatures (in °C per decade) over summers (June-July-
833 August) in 1981–2079. Each dot represents one studied city. The error bars indicate the 12-member ensemble
834 spread of UKCP18-regional. Red dots show trends in summer daily maximum temperature, whereas blue dots
835 show trends in summer daily minimum temperature. The dashed line shows the identity line.

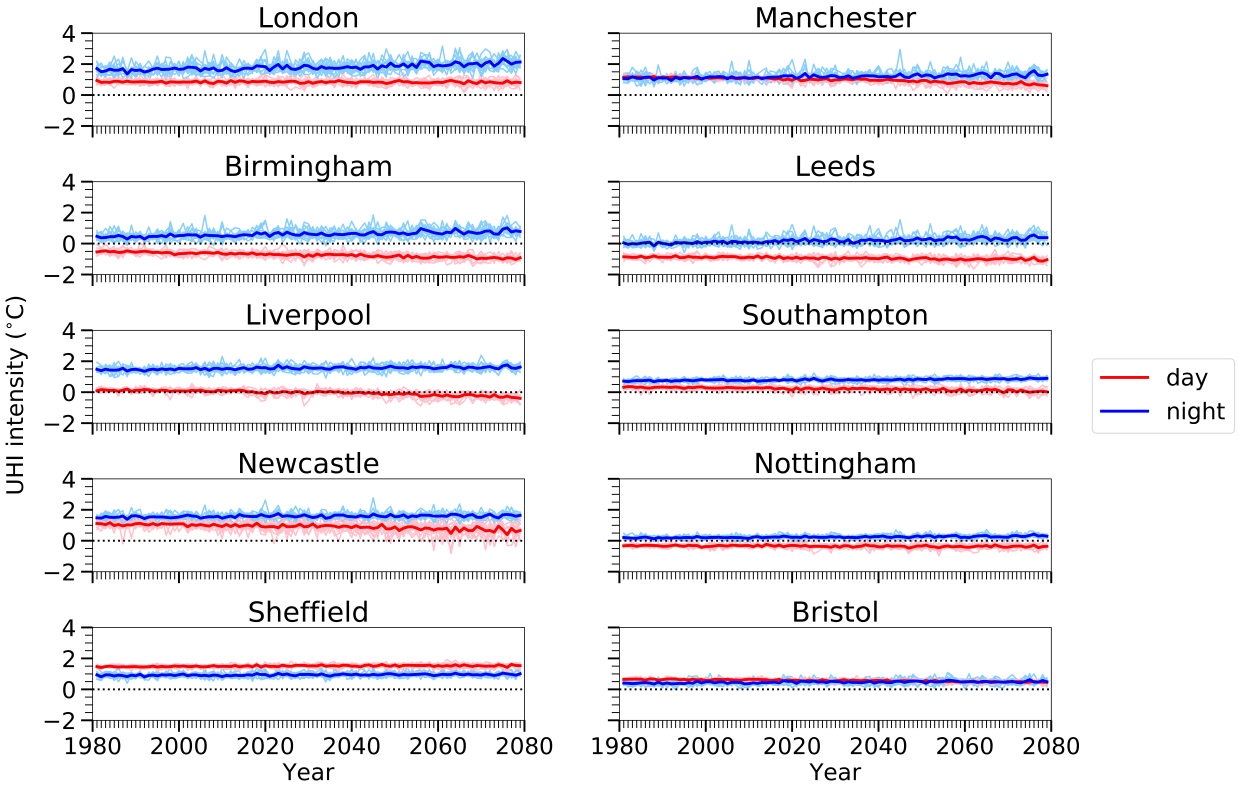

836 FIG. 3. Time evolution of bias-corrected summer (June-July-August) daytime (red) and night-time (blue) UHI
837 intensities from UKCP18-regional during 1981–2079. Thick lines indicate the ensemble means, whereas thin
838 lines indicate individual ensemble members.

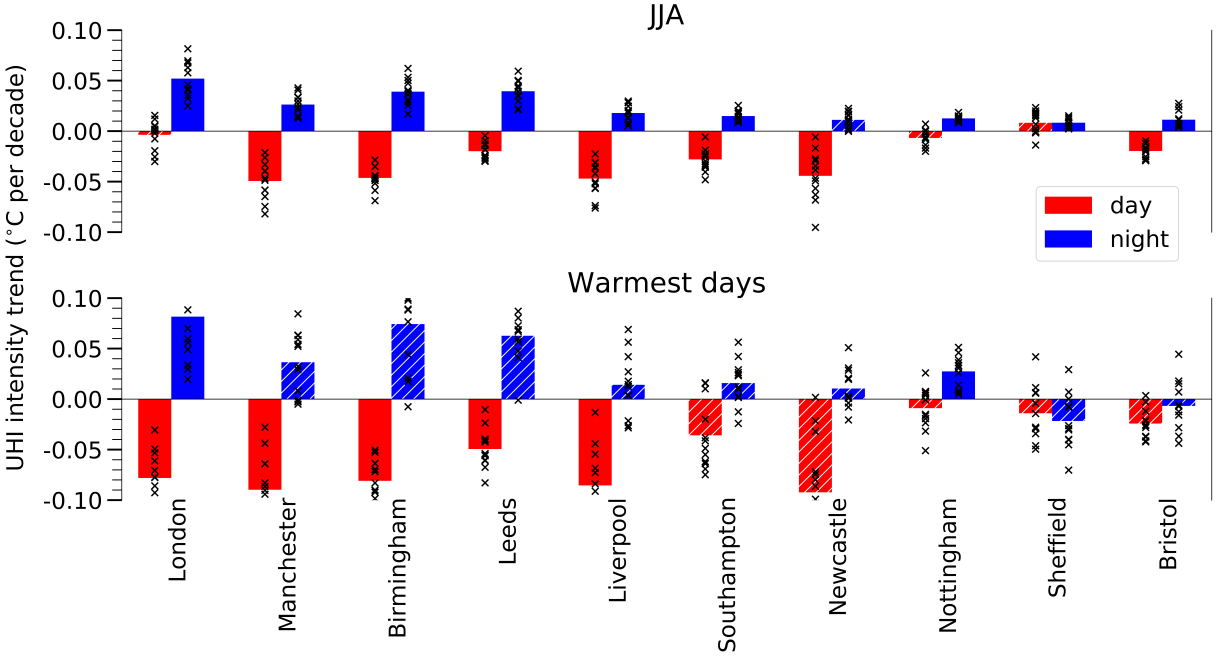

FIG. 4. UHI intensity trends (in °C per decade) in 1981–2079 for daytime (red) and night-time (blue) near-surface air temperatures. The bars show the UKCP18-regional ensemble-mean values whereas the crosses indicate individual ensemble members. Bars where the 12-member ensemble range crosses zero are hatched. The upper panel shows trends in summer (June-July-August), whereas the bottom panel shows trends in UHI intensities on annual three consecutive warmest days.

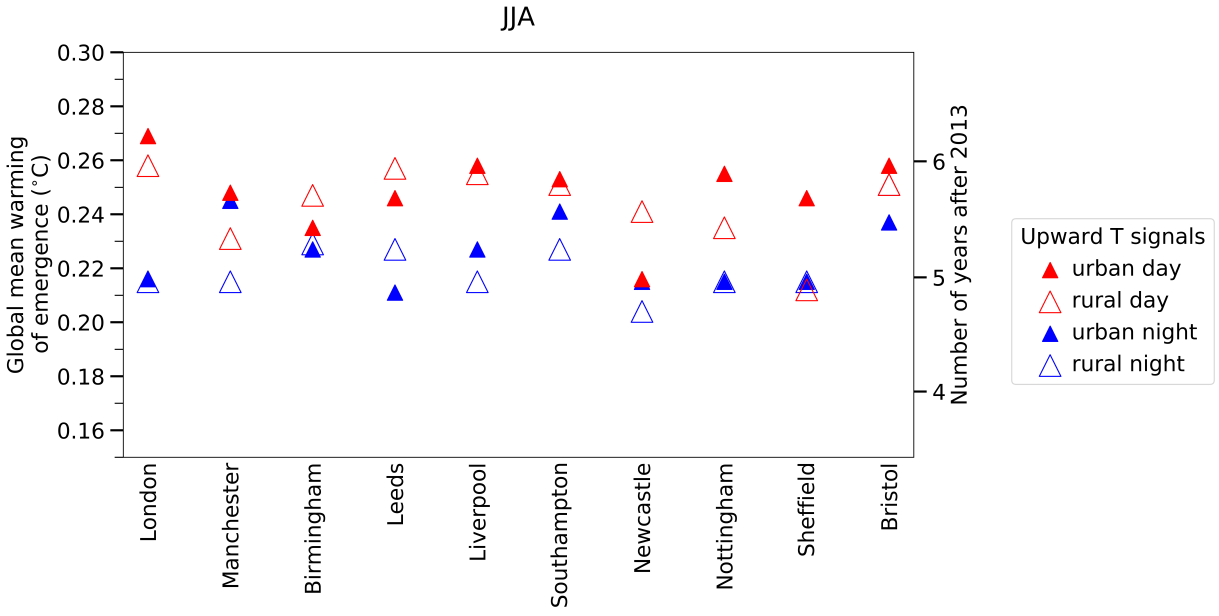

844 FIG. 5. Global mean warming of emergence of summer daytime (red) and night-time (blue) urban (filled
845 triangles) and rural (empty triangles) temperature signals in and around the 10 most populous cities in England.
846 All signals are positive as indicated by the upward triangles. Warming of emergence is measured in global mean
847 warming in °C since 2008–2018. The right vertical axis shows the corresponding number of years after 2013 (the
848 middle year of the 2008–2018 baseline), based on the ensemble mean of the UKCP18-global simulations. 1.5°C
849 global warming above pre-industrial levels corresponds to 0.53°C warming since the average of 2008–2018,
850 which is above the vertical scale of this figure.

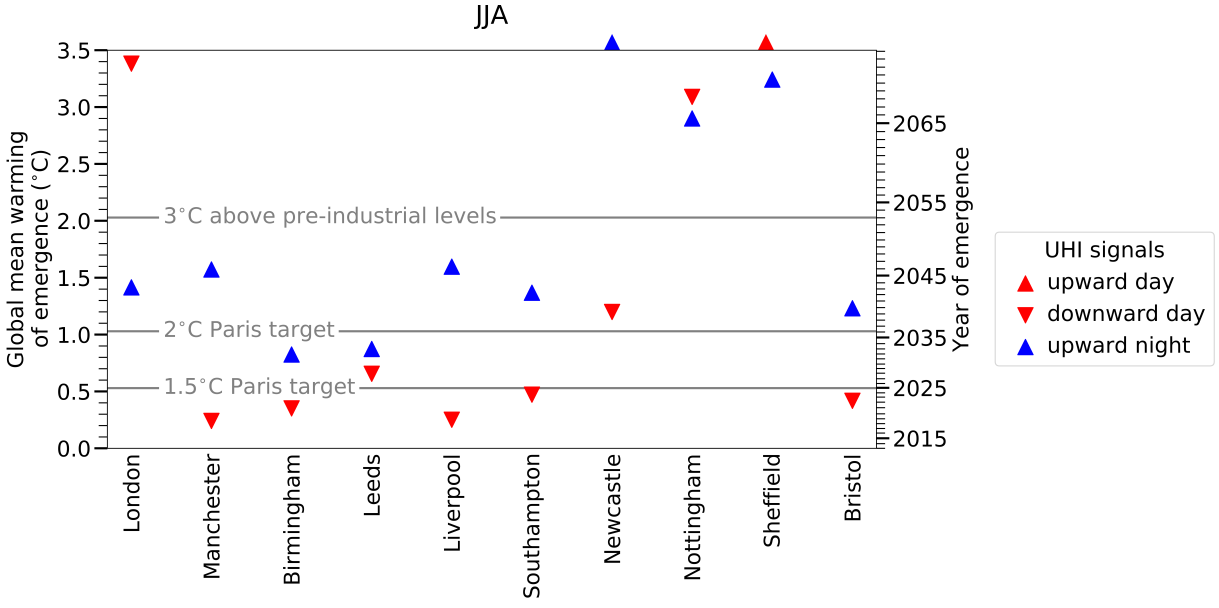

FIG. 6. Global mean warming of emergence of summer daytime (red) and night-time (blue) UHI signals in the 10 most populous cities in England. Upward triangles indicate positive (upward) signals, whereas downward triangles indicate negative (downward) signals. Warming of emergence is measured in global mean warming in °C since 2008–2018. The right vertical axis shows the corresponding year of emergence based on the ensemble mean of the UKCP18-global simulations. The grey horizontal lines indicate the Paris Agreement temperature targets and 3°C global warming above pre-industrial levels (1850–1900), based on the UKCP18-global simulations and global mean warming between 1850–1900 and 2008–2018 in HadCRUT4-CW. Triangles on top of the figure indicate daytime (red) and night-time (blue) UHI changes that do not emerge in the UKCP18 simulations.

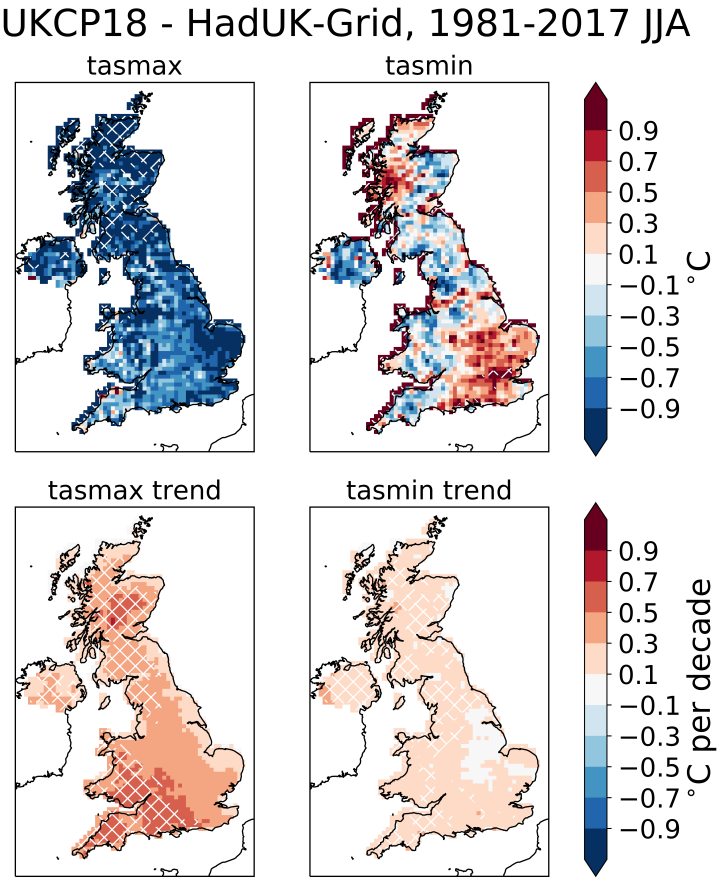

Fig. A1. Differences between UKCP18-regional ensemble mean and HadUK-Grid over summers (June-July-August) in 1981–2017. The top panel shows biases in average daily maximum (left) and minimum (right) temperatures, whereas the bottom panel shows biases in their trends in °C per decade. Hatching indicates areas where HadUK-Grid falls outside of the UKCP18-regional ensemble range.

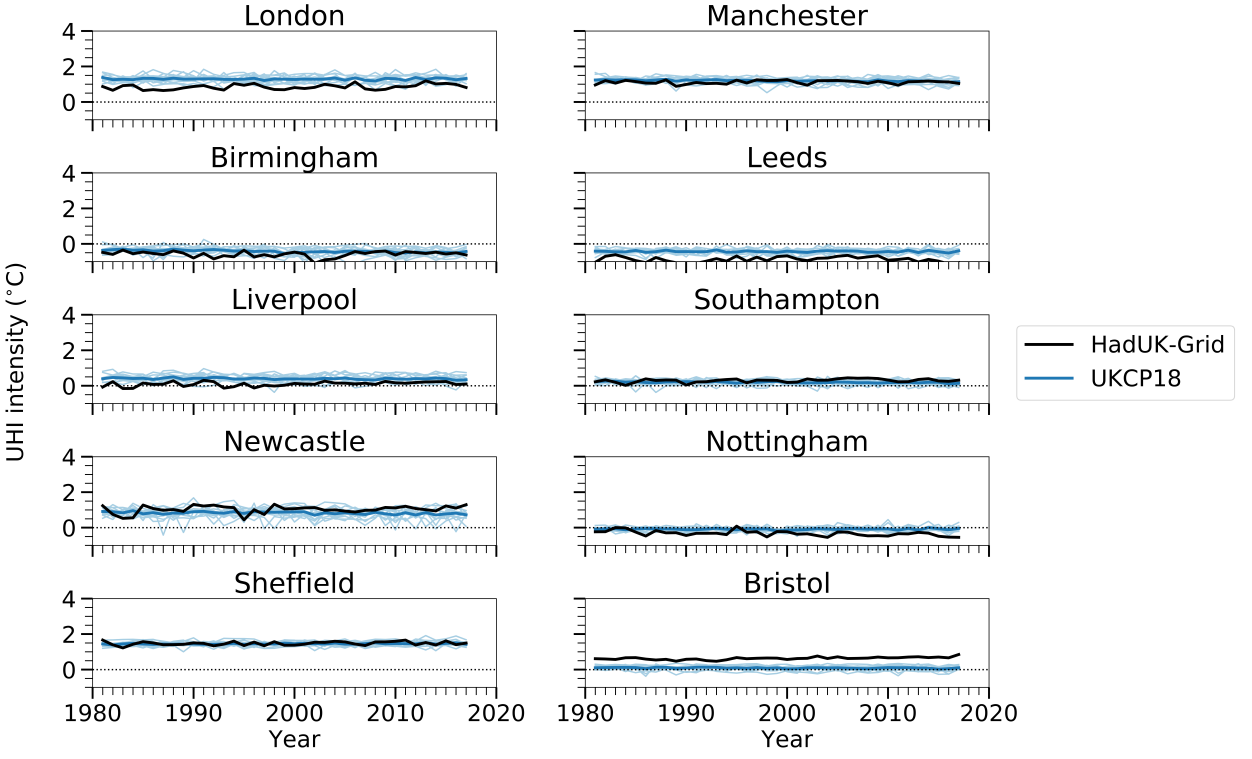

Fig. A2. Time evolution of summer (June-July-August) daytime UHI intensities in HadUK-Grid (black line) and the UKCP18-regional simulations (blue lines) during 1981–2017. Thick blue lines indicate UKCP18-regional ensemble means, whereas thin blue lines indicate individual ensemble members.

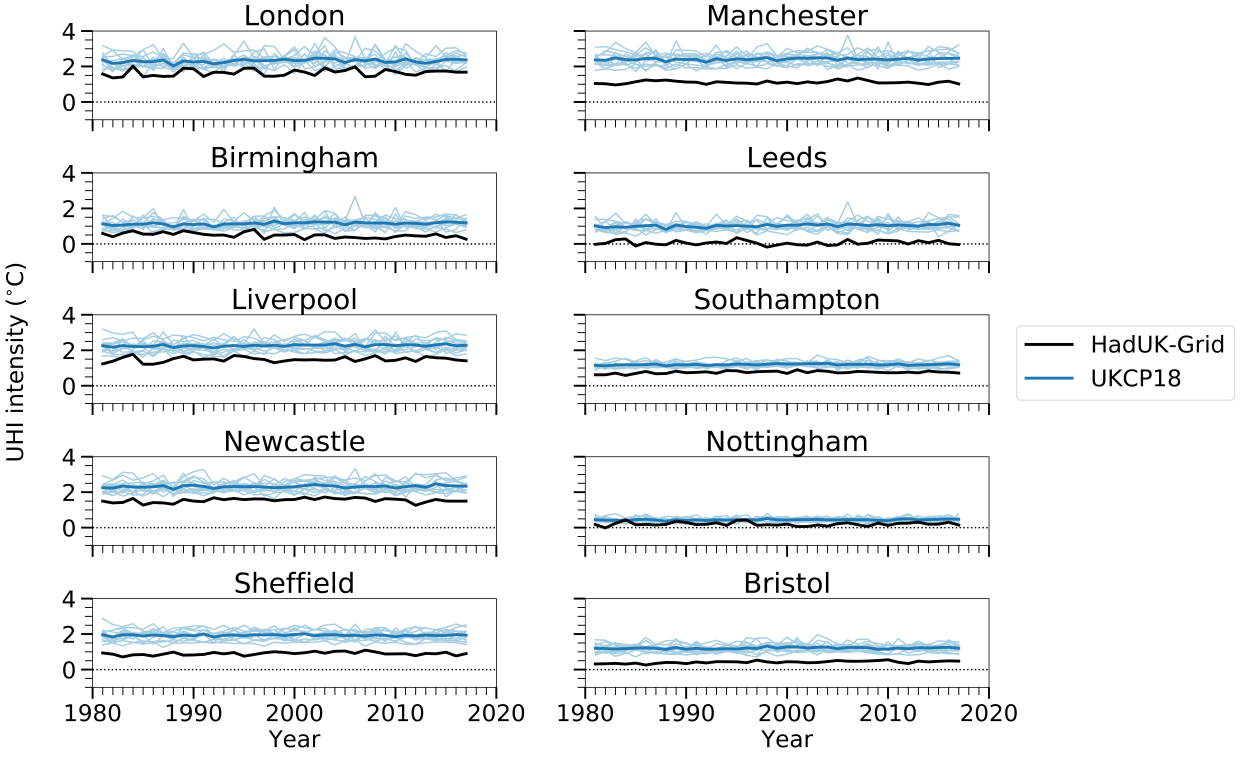

Fig. A3. Time evolution of summer (June-July-August) night-time UHI intensities in HadUK-Grid (black line) and the UKCP18-regional simulations (blue lines) during 1981–2017. Thick blue lines indicate UKCP18-regional ensemble means, whereas thin blue lines indicate individual ensemble members.

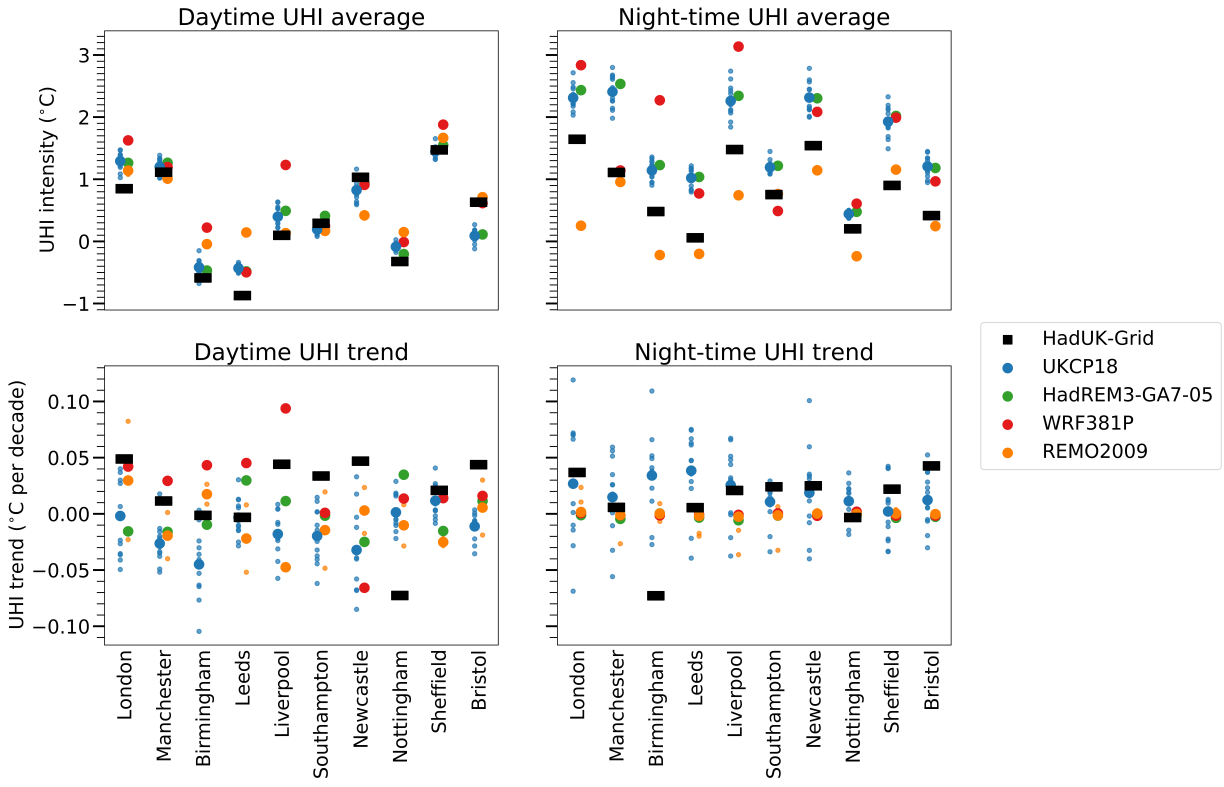

Fig. A4. Comparisons of 1981–2017 summer (June-July-August) UHI intensities (top panel) and trends (bottom panel) between HadUK-Grid (black rectangles), UKCP18-regional (blue dots), and three regional climate models in the EURO-CORDEX experiment (green dots for HadREM-GA7-05, red dots for WRF381P and orange dots for REMO2009). The left panel shows daytime UHIs, and the right panel shows night-time UHIs. Small dots indicate results from individual ensemble members, whereas big dots indicate the ensemble means.

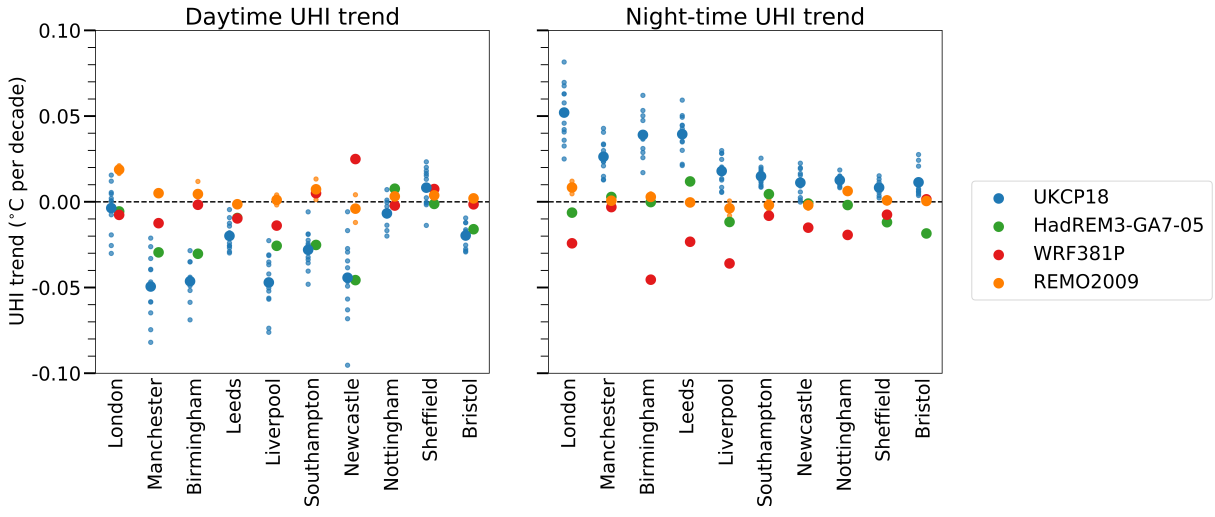

Fig. A5. Comparisons of 1981–2079 summer (June-July-August) UHI intensity trends between UKCP18-regional (blue dots) and three regional climate models in the EURO-CORDEX experiment (green dots for HadREM-GA7-05, red dots for WRF381P and orange dots for REMO2009). The left panel shows daytime UHI trends, and the right panel shows night-time UHI trends. Small dots indicate results from individual ensemble members, whereas big dots indicate the ensemble means.